Received: 24 June 2020 | Revised: 9 September 2020 | Accepted: 25 September 2020

DOI: 10.1049/ote2.12012

IET Optoelectronics

The Institution of Engineering and Technology WILEY

ORIGINAL RESEARCH PAPER

Reduction-controlled graphene oxide saturable absorbers and its effect on ultrashort Er-doped fibre laser

Mohd Afiq Ismail[1] | **Mohd Zulhakimi Abdul Razak**[2] | **Sulaiman Wadi Harun**[3] | **Abdul Manaf Hashim**[1]

[1]Advanced Devices and Material Engineering, Malaysia-Japan International Institute of Technology, Universiti Teknologi Malaysia, Kuala Lumpur, Malaysia

[2]Institute of Microengineering and Nanoelectronics, Universiti Kebangsaan Malaysia, Bangi, Selangor, Malaysia

[3]Department of Electrical Engineering, Faculty of Engineering, University of Malaya, Kuala Lumpur, Malaysia

Correspondence

Mohd Afiq Ismail, Advanced Devices and Material Engineering, Malaysia-Japan International Institute of Technology, Universiti Teknologi Malaysia, Kuala Lumpur 54100, Malaysia.
Email: mohd.afiq@utm.my

Funding information

Universiti Teknologi Malaysia, Grant/Award Number: PY 2018/02912

Abstract

The authors controlled the reduction of three graphene oxide (GO) saturable absorber (SA) thin films by controlling the exposure time under a solar simulator and afterwards, incorporated them into an Er-doped fibre laser in order to investigate their effect on ultrashort pulse. The authors also hypothesized that the controlled reduction would result in a controlled absorption, and ultimately, a controlled modulation depth. A larger modulation depth would lead to stronger pulse shaping and shorter pulse duration. Sample A was left unreduced, whereas samples B and C were exposed for 15 and 30 min, respectively. Afterwards, their modulation depths were measured using twin-detector method and determined to be 0.69%, 1.2% and 1.94%, respectively. When used as an SA in an Er-doped fibre laser, the result showed pulse duration shortening; from 670 to 520 fs, as well as spectral broadening; from 4.22 to 6.73 nm. In addition, we also observed changes in repetition rate, output power and time-bandwidth product (TBP). The result of this paper shows the feasibility of controlling the modulation depth of a GO SA and conclusively shows the effect of modulation depth on ultrashort pulse.

1 | INTRODUCTION

Since the demonstration of graphene as saturable absorber (SA) [1], other research groups have discovered other 2D materials with Pauli blocking property and ultrafast recovery time. Black phosphorus [2,3], transition metal dichalcogenides (TMD) [4,5] and topological insulator (TI) [6,7], are examples of 2D materials that have been fabricated into SA and then used to generate passive Q-switched and ultrashort fibre lasers. Each of these materials have their own advantage, for example, graphene has ultrabroadband absorption [8], whereas black phosphorus can change its bandgap depending on the number of layers [9]. Compared to earlier type of SA like semiconductor saturable absorber mirror (SESAM) [10,11], 2D materials based SA are economical and easy to fabricate.

The effect of modulation depth on ultrashort pulse has been theoretically discussed in Refs. [12] and [13]. There have been few publications that, to some extent, demonstrate the effect of modulation depth on ultrashort pulse. For example, the authors in Ref. [14] compared the ultrashort pulse performance between graphene oxide (GO) and reduced GO (rGO) SA and found that there was no change in pulse durations between the SAs, although their modulation depths differ by 3%. Nevertheless, there was a slight variance in full width at half maximum bandwidth and time-bandwidth product (TBP). The authors concluded that 'there is no significant difference in the laser performance between the investigated SA'. In another paper, the authors fabricated a few samples of graphene SA with varying number of layers to achieve a scalable modulation depth [15]. Increasing the number of graphene layers deliberately increases the absorption and as a result, increases the modulation depth. Higher modulation depth is expected to lead to stronger and shorter pulse duration. However, for both papers, the authors took measurements at a different pump power for each sample, thus, the influence of pump power over the ultrashort laser performance could not be ignored. Therefore, the influence of modulation depth over ultrashort pulse was inconclusive. In

contrast, Ref. [1] reported that an increase in the number of graphene layer would result in a decrease of modulation depth due to the increase in non-saturable loss caused by enhanced scattering of graphene layers. Nevertheless, both papers showed that by varying the number of graphene layers, a scalable modulation depth can be achieved. Graphene that was used in Refs. [1,15] was grown using chemical vapour deposition (CVD) method. Although the method can produce a high-quality solid material, its disadvantages include high deposition temperature, toxic precursor and dangerous by-product. In Ref. [16], the authors compared ultrashort pulse characteristics using several 2D materials with different modulation depth and saturation intensity. Their findings show that as the modulation depth of an SA increase, pulse duration decrease and 3-dB bandwidth increase. Yet, since the authors compared between several 2D materials, the paper does not highlight modulation depth as a controllable parameter.

Authors in Ref. [17,18] fabricated multiple types of 2D materials SA using few-layer spin coating approach in order to finely tune their characteristics. They reported that as the layers increase, so does the saturation intensity and modulation depth. This fabrication method does allow for a scalable modulation depth yet less complicated than the CVD method.

Traditionally, GO serves as a precursor to graphene. Other than carbon, GO contains epoxy, hydroxyl, carbonyl and carboxyl groups, but the content of epoxy and hydroxyl groups is the key to reducing GO. By carefully reducing the oxygen content in GO, there exist a possibility of tailoring its electrical and optical properties [19,20]. Reducing GO can be performed using several methods; chemically [21,22], thermally [23–25], by solar irradiation [26,27] and also by 'green reductants' [28–30]. Reducing GO increases its absorbance while the bandgap can be tuned from 2 to 0.02 eV [31]. Hence, it allows GO to operate from visible to near-infrared (NIR) bands. Moreover, Z-scan and femtosecond pump-probe measurements had shown that GO possesses saturable absorption property as well as ultrafast carrier dynamic in the order of 0.1 ps, comparable to graphene [32–34].

The objective of this paper is twofold. First is to demonstrate the feasibility of controlling the modulation depth of GO SA by controlling its reduction using a solar simulator. Controlling the reduction by controlling the exposure time would result in a controlled absorbance and ultimately, a controlled modulation depth. Second is to demonstrate the effect of modulation depth on ultrashort pulse. Our methodology demonstrates a safe, economical and easy method of controlling the modulation depth and present a conclusive evidence regarding the effects of modulation depth on ultrashort pulse.

2 | GO SA FABRICATION AND CHARACTERIZATION

The GO that was used in this experiment was synthesized by using Hummers method [35], started with mixing 3 g of graphite flakes with 18 g of potassium permanganate powder. The powder mixture was added into 360 ml of sulphuric acid (95 wt.%) and 40 ml of phosphoric acid (85 wt.%). The process caused an exothermic reaction. Afterwards, the mixture was heated at 50°C on a hot plate while constantly stirred using a magnetic stirrer at 300 rpm, for the duration of 18 h. In order to stop the oxidation, the solution was cooled down to 27°C and later poured into a cooled 400 ml of deionised (DI) water, mixed with 30 ml of hydrogen peroxide (30 wt.%). Next, the solution was centrifuged at 4000 rpm for 1 h, which separated the solution into supernatant and infranatant. The infranatant was taken and washed 3 times by using an equal mixture of hydrochloric acid (20 wt%) and DI water, for the purpose of removing the remaining potassium salt. Finally, the infranatant was dispersed in DI water (final concentration = 2 mg ml^{-1}) to produce a dispersed GO solution.

In order to characterize our GO using Raman spectroscopy, we dried few drops of GO solution onto a glass slide. Figure 1 shows Raman shift when measured using 514 nm laser. The result shows a D-peak (1359 cm^{-1}) due to the breathing mode of aromatic rings, which usually an indication of defect [36]. Another peak at 1597 cm^{-1} (G-peak), arise due to doubly degenerate phonon mode (E_{2g}) at the Brillouin zone centre and indicate the existence of sp^2 carbon networks. The 2D region corresponds to the overtone of the D band and believed to be induced by disorder [37]. The value of integrated intensity ratio (I_D/I_G), which is commonly used for quantifying defect in graphitic materials, is 1.03. The dominant D-peak arise due to attachment with functional group such as hydroxyl, epoxy on the carbon skeleton [38].

An amount of 20 ml of GO solution was used to fabricate GO-PVA thin film. The solution was sonicated for 1 h in a 37 kHz ultrasonic bath and, afterwards, was placed onto a hot plate and stirrer at 600 rpm using a magnetic stirrer. An approximately 250 mg of PVA granules were added slowly into the whirlpool, avoiding the vortex. In past papers, PVA was chosen as a host for a variety of 2D materials based SA due to its transparency, safety, flexibility and ease of use [39–41]. The whirlpool was slowly heated to 90°C and maintained for 30 min. This was to ensure that the PVA granules were fully

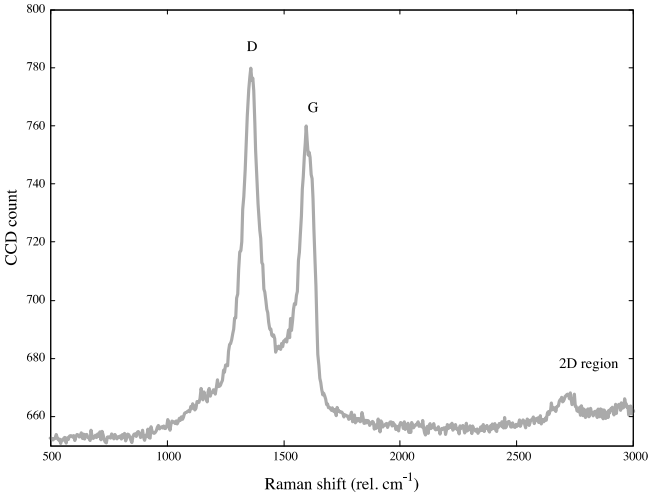

FIGURE 1 Raman spectroscopy of graphene oxide

dissolved into the solution. The process was followed by drying in an oven at 50°C for 11 h. The thickness of the sample was measured to be 82 μm.

The fabricated GO SA thin film was cut into three equal parts, which will be known henceforth as samples A, B and C. Sample A was left unreduced, whereas samples B and C were irradiated by a 100 W solar simulator, for 15 and 30 min, respectively. This reduction method was chosen due its effectiveness and simplicity – the GO can be reduced in its thin film form. Later, insertion loss measurements were performed on all samples using a tuneable C-band laser. As a result, the insertion loss of samples A, B and C was determined to be 2.53, 2.85 and 3.05 dB, respectively. The reduction time of GO SA needs to be carefully controlled as high insertion loss could render the laser to operate in Q-switching regime instead. Based on our experience, by irradiating the SA under solar simulator for 45 min, the mode-locking condition in our laser could no longer be guaranteed.

The modulation depth of our samples was measured using twin-detector method, as depicted in Figure 2. For this purpose, an ultrashort Er-doped fibre (EDF) laser was developed in-house using non-linear polarization rotation (NPR) technique. The laser had a pulse duration of 580 fs, a repetition rate of 16.75 MHz and a maximum output power of ~10 dBm. The output from the laser was connected to a 23-dB variable optical attenuator and later, divided by an output coupler (OC). Ninety per cent of the output power was channelled into the SA, while the remaining 10% was used as reference.

The result of the measurement was then fitted into the following equation [42]:

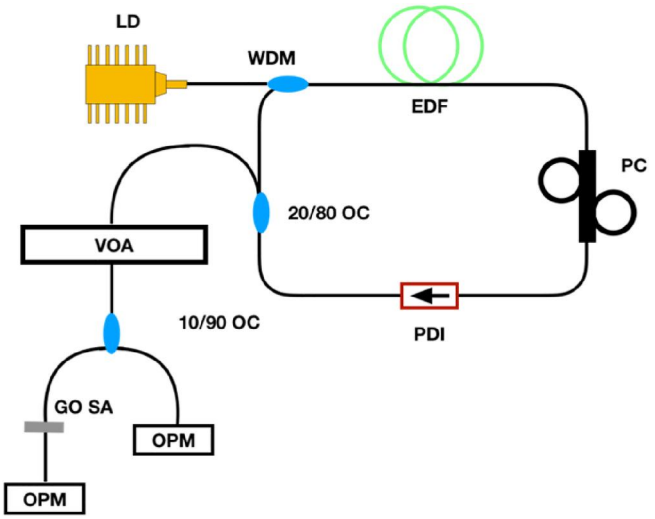

FIGURE 2 Modulation depth measurement set-up. LD, 980 nm laser diode; WDM, 980/1550 wavelength division multiplexer; EDF, Er-doped fibre; PC, polarization controller; PDI, polarization-dependent isolator; 20/80 OC, 20/80 output couple;, VOA, variable optical attenuator; ,0/90 OC: 10/90 output coupler; GO SA, graphene oxide saturable absorber; OPM, optical power meter

$$\alpha(I) = \frac{\alpha_{\text{sat}}}{1 + \frac{I}{I_{\text{sat}}}} + \alpha_{\text{ns}} \quad (1)$$

where, $\alpha(I)$ is the absorption coefficient, α_{sat} is the saturable absorption, I is the intensity, I_{sat} is the saturable intensity and α_{ns} is the non-saturable absorption. Result of the fitting (Figure 3) shows that samples A, B and C have a modulation depth of 0.69%, 1.2% and 1.94%, respectively. In addition, the saturation intensity of samples A, B and C was 0.00011, 0.00008 and 0.0002 mJ cm^{-2}, respectively. The large value of α_{ns} could originate from scattering loss due to large GO particles that were present in the SA thin film since the GO solution was not subjected to centrifugation before stirring. We also believe that the measurements were limited by the maximum attenuation value of our VOA (23 dB). Furthermore, the value of modulation depth can also change depending on pulse duration and pulse energy used in the measurement. Reference [43] demonstrated that higher percentage of modulation depth and saturation intensity can be obtained by using higher pulse energy and/or shorter pulse.

3 | EXPERIMENTAL SET-UP

Figure 4 shows the experimental set-up for the generation of EDF laser. The ring laser was pumped by a 980 nm laser diode (LD), with a maximum pumping power of 500 mW. The pump laser was channelled into the laser cavity via a 980/1550 nm wavelength division multiplexer (WDM). The common port of the WDM was spliced to a gain medium – a 0.8-m EDF with Erbium ion concentrations of 2000 ppm. The gain medium has a cut-off wavelength of 900–970 nm with numerical aperture (NA) between 0.23 and 0.26. At 1531 nm, the gain medium has an absorption of 35 to 45 dB/m. A polarization insensitive (PI), single-stage fibre isolator was spliced after the gain medium to ensure unidirectional propagation. The laser resonator's slope efficiency was measured at 7.9%.

A small cut of GO SA thin film, which act as a mode-locker was sandwiched between two fibre ferrules, was

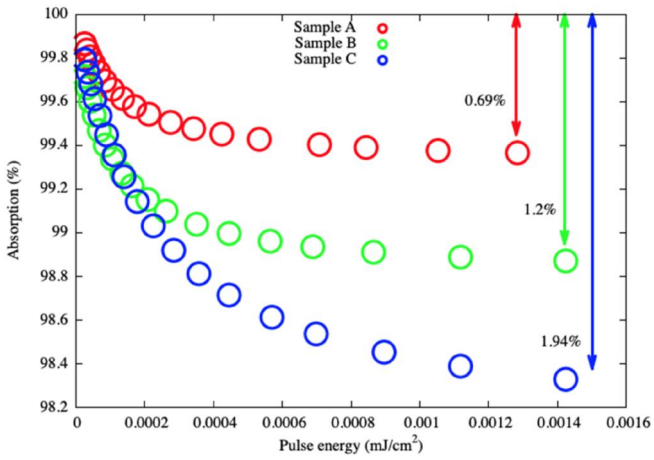

FIGURE 3 Modulation depth result after fitted with Equation (1)

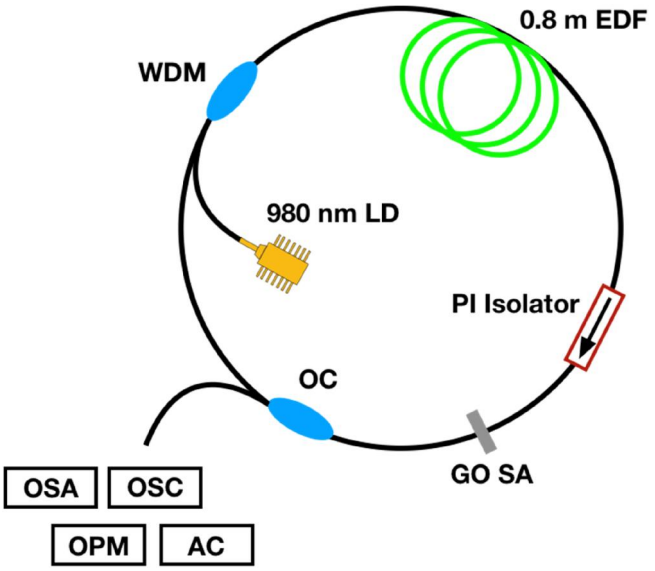

FIGURE 4 LD, laser diode; WDM, 980/1550 wavelength division multiplexer; EDF, Er-doped fibre; PI isolator. polarization-independent isolator; OC, 20/80 output coupler; GO SA, graphene oxide saturable absorber; OSA, optical spectrum analyser; OSC, oscilloscope; AC, autocorrelator; OPM, optical power meter

incorporated into the cavity between the isolator and OC. An amount of 20% of the total intracavity power was extracted through a 20/80 OC into measuring instruments such as optical spectrum analyser (OSA), digital oscilloscope (OSC), autocorrelator (AC) and optical power meter (OPM).

The optical spectrum and ultrashort signal were monitored and measured using OSA and OSC, respectively. A two-photon absorption AC was used to measure the pulse duration, whereas OPM measured the laser output power. Except for the gain medium, the laser ring cavity was composed of SMF-28 single-mode fibre. As there were neither polarization-dependent component nor polarization controller were used in the cavity, the possibility that the ultrashort pulse had originated from NPR was eliminated.

The total length of the cavity was ~8.3 m (cavity round-trip time = 27.8 ns), which comprised normal and anomalous dispersion fibres. Given that the chromatic dispersion coefficient, D, for the gain medium at 1550 nm is −21.64 ps $nm^{-1}km^{-1}$, a 0.8-m EDF has a dispersion of −0.02 ps nm^{-1}. The dispersion of SMF-28, however, is anomalous at 1550 nm, with D value of 17 ps nm^{-1} km^{-1}. Therefore, 7.5 m of SMF-28 resulted in a chromatic dispersion of 0.13 ps nm^{-1}. When combined, the total cavity dispersion, D_{total} is 0.11 ps nm^{-1}. Based on the total cavity dispersion value, the ultrashort laser was operating in the soliton regime [44–46].

4 | RESULTS AND DISCUSSION

In the experiment, only one laser cavity was used, without any adjustment between measurements, therefore, maintaining the total cavity dispersion. The fibre laser has a lasing threshold of 8.7 mW. In order to demonstrate that the pulse duration shortening was influenced by the modulation depth alone, all measurements were recorded at pump power = 30 mW. All ultrashort pulses self-started, with slight variation in power. For example, sample A self-started at 26.8 mW, whereas samples B and C self-started at 31.3 mW. For sample A, the pump power was increased to 30 mW, whereas for samples B and C, the pump power was reduced to 30 mW before any measurement was recorded.

The optical spectra and pulse evolution can be observed from Figure 5. As the figure shows, the optical spectrum of samples A, B and C broadened from 4.22 nm to 4.52 nm to 6.73 nm, respectively. In contrast, the corresponding pulse duration decreased from 670 fs to 580 fs to 520 fs. This is depicted more clearly in Figure 6. The relationship between pulse duration and spectral bandwidth can be explained using Fourier transform, whereby, when a signal is compressed in the time domain, it is spread out in the frequency domain.

The optical spectrum of sample A shows a continuous wave component which may originate from an overdriven pump power (sample A self-started at 26.8 mW but the measurement was taken at 30 mW). Figure 5 also shows that the centre wavelength, λ_{centre}, shifted to shorter wavelength (e.g. sample A: 1558.29 nm, sample B: 1557.94 nm, sample C: 1556.73 nm). Similar observation was also noticeable in Ref [15]. Furthermore, Kelly sideband amplitudes becomes more prominent because pulse duration became shorter [47].

During experiment, we also noticed changes in repetition rate between samples, despite maintaining the same cavity length. The repetition rate increased as the measurements progress from sample A to sample C (from 25.07 to 25.2 MHz). These changes were attributed to the change in central wavelength which shifted to shorter wavelength. Shorter wavelength has lower effective group index of refraction (EIOR), which resulted in higher repetition rate. Figure 7 further illustrates the changes between central wavelength and its corresponding repetition rate.

Our measurements showed TBP values of more than 0.315 (bandwidth-limited $sech^2$ value). The TBP value is expected to increase with increasing modulation depth, as simulated by [48]. From Figure 8, the TBP for sample B is lower than samples A and C. We suspect that, since the measurement of sample A was taken at a pump power slightly higher than its pulsing threshold, the effect from self-phase modulation (SPM) broadened the optical spectrum and subsequently increased the value of TBP.

The output power, P_{out}, from the laser also changed with each sample, regardless of using the same pump power when performing all measurements. For samples A, B, C, the output was 0.482, 0.434 and 0.242 mW, respectively. The decrease in output power was due to the increase in insertion loss of the samples.

In general, the ultrashort pulse performance of each samples can be summarized in Table A1 (see Appendix 1).

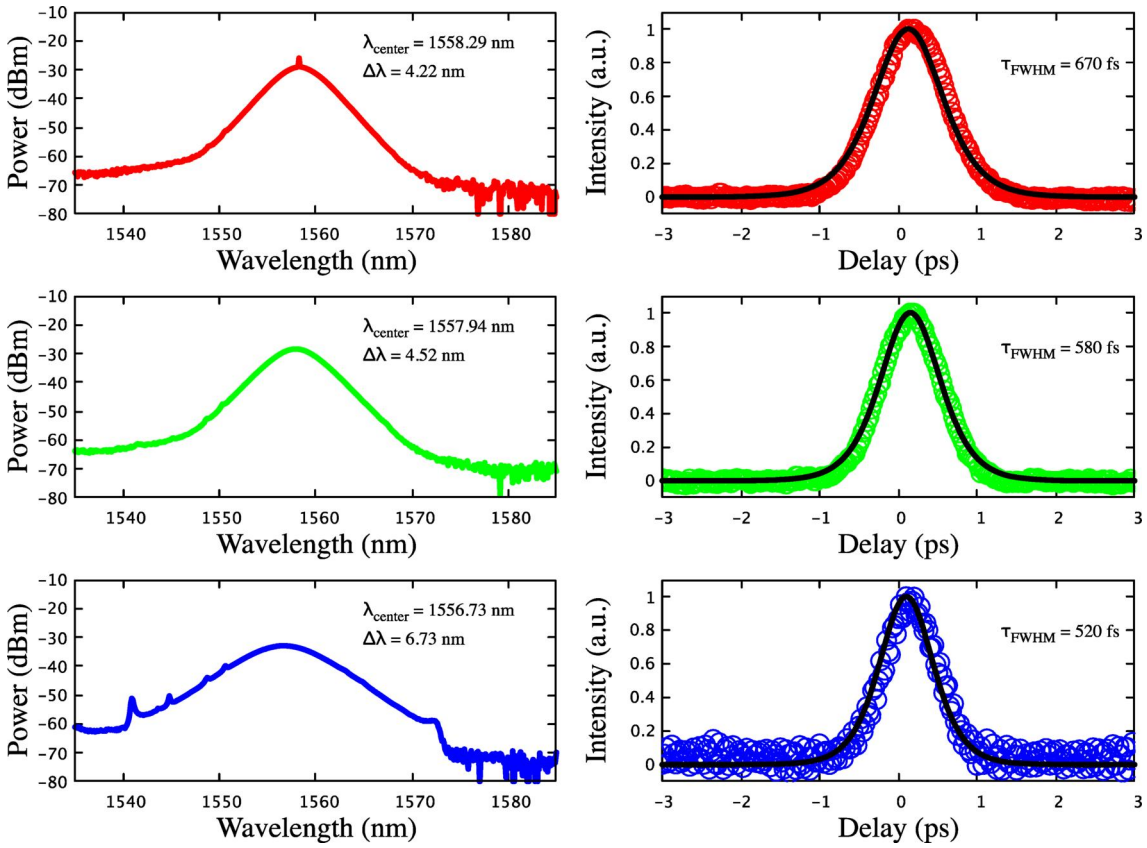

FIGURE 5 Measured optical spectra and their corresponding pulse duration for samples A (red), B (green) and C (blue)

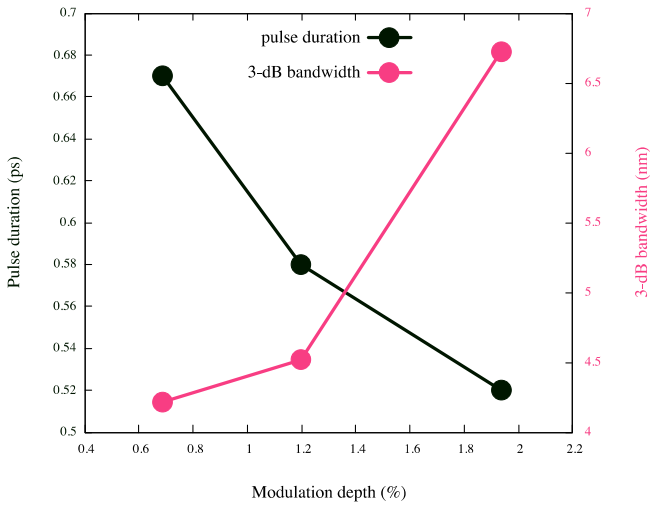

FIGURE 6 3-dB bandwidth broadening and pulse duration shortening for sample with relation to modulation depth

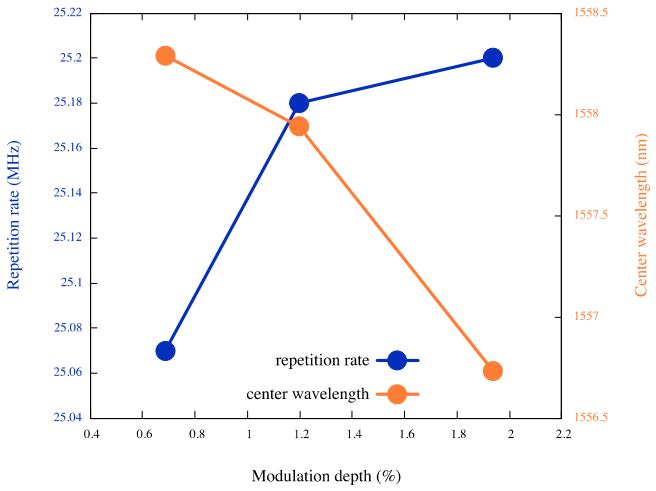

FIGURE 7 Shift in repetition rate and centre wavelength according to modulation depth

In terms of stability, samples A, B and C exhibited excellent signal-to-noise ratio (SNR) of 59.57, 55.49 and 48.89 dB, respectively. Although larger modulation depth is often associated with better SNR, in this case, a larger modulation depth is also associated with larger insertion loss. Furthermore, the SNR of samples B and C was taken at a lower pump power (30 mW) than their pulsing threshold (31.3 mW). These factors might contribute to lower SNR.

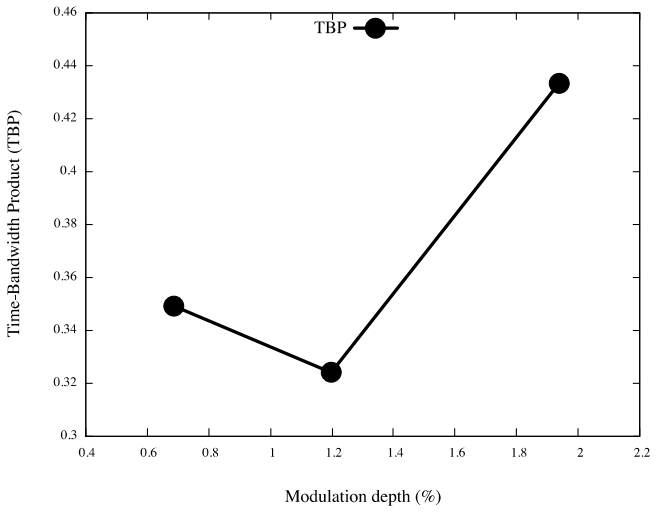

FIGURE 8 Time-bandwidth product change with modulation depth

5 | CONCLUSION

As a conclusion, we have successfully demonstrated a safe, economical and easy way of controlling the modulation depth of a GO SA and conclusively presented the effect of modulation depth on ultrashort pulse. The modulation depth of a GO SA can be controlled by controlling the reduction time. An increase in the reduction time will result in an increase in absorption, which will increase the modulation depth. After the SAs were exposed for 15 and 30 min, the modulation depth of our samples increased from 0.69% (no exposure) to 1.2% to 1.94%. Larger modulation depth GO SA had shortened the pulse duration, broadened the 3-dB bandwidth, increased the repetition rate and lowered the output power. The finding of this paper offers alternative route to pulse duration shortening and spectral broadening, and can potentially find its usefulness in telecommunication, metrology and sensing.

ACKNOWLEDGEMENT

We wish to thank Mr Haziq Aiman at the photonics lab in the University of Malaya for his assistance.

ORCID

Mohd Afiq Ismail https://orcid.org/0000-0001-5208-0813

REFERENCES

1. Bao, Q., et al.: Atomic-layer graphene as a saturable absorber for ultrafast pulsed lasers. Adv. Func. Mater. 19(19), 3077–3083 (2009)
2. Chen, Y., et al.: Mechanically exfoliated black phosphorus as a new saturable absorber for both Q-switching and mode-locking laser operation. Opt. Express. 23(10), 12823–12833 (2015)
3. Sotor, J., et al.: Black phosphorus saturable absorber for ultrashort pulse generation. Appl. Phys. Lett. 107(5), 051108-1–051108-5 (2015)
4. Mao, D., et al.: Passively Q-switched and mode-locked fiber laser based on an Res2 saturable absorber. IEEE J. Sel. Top. Quant. Electron. 24(3), 1–6 (2018)
5. Woodward, R., Kelleher, E.: 2d saturable absorbers for fibre lasers. Appl. Sci. 5(4), 1440–1456 (2015)
6. Luo, Z.C., et al.: 2 Ghz passively harmonic mode-locked fiber laser by a microfiber-based topological insulator saturable absorber. Opt. Lett. 38(24), 5212–5215 (2013)
7. Zhao, C., et al.: Ultra-short pulse generation by a topological insulator based saturable absorber. Appl. Phys. Lett. 101(21), 211106-1–211106-4 (2012)
8. Nair, R.R., et al.: Fine structure constant defines visual transparency of graphene. Science. 320(5881), 1308 (2008)
9. Liu, H., et al.: Phosphorene: an unexplored 2d semiconductor with a high hole mobility. ACS Nano. 8(4), 4033–4041 (2014)
10. Keller, U., Tropper, A.C.: Passively modelocked surface-emitting semiconductor lasers. Phys. Rep. 429(2), 67–120 (2006)
11. Okhotnikov, O., Grudinin, A., Pessa, M.: Ultra-fast fibre laser systems based on SESAM technology: new horizons and applications. New J. Phys. 6, 177 (2004)
12. Haus, H.A.: Mode-locking of lasers. IEEE J. Sel. Top. Quant. Electron. 6(6), 1173–1185 (2000)
13. Renninger, W.H., Wise, F.W.: Fundamental limits to mode-locked lasers: toward terawatt peak powers. IEEE J. Sel. Top. Quant. Electron. 21(1), 63–70 (2015)
14. Sobon, G., et al.: Graphene oxide vs. reduced graphene oxide as saturable absorbers for Er-doped passively mode-locked fiber laser. Opt. Express. 20(17), 19463–19473 (2012)
15. Sobon, G., et al.: Multilayer graphene-based saturable absorbers with scalable modulation depth for mode-locked ER- and TM-doped fiber lasers. Opt. Mater. Express. 5(12), 2884–2894 (2015)
16. Xu, H., et al.: Effects of nanomaterial saturable absorption on passively mode-locked fiber lasers in an anomalous dispersion regime: simulations and experiments. IEEE J. Sel. Top. Quant. Electron. 24(3), 1–9 (2018)
17. Jiang, X., et al.: Bismuth telluride topological insulator nanosheet saturable absorbers for Q-switched mode-locked Tm:Zblan waveguide lasers. Ann. Phys. 528(7–8), 543–550 (2016)
18. Jiang, X., et al.: Low-dimensional nanomaterial saturable absorbers for ultrashort-pulsed waveguide lasers. Opt. Mater. Express. 8(10), 3055–3071 (2018)
19. Eda, G., Chhowalla, M.: Chemically derived graphene oxide: towards large-area thin-film electronics and optoelectronics. Adv. Mater. 22(22), 2392–2415 (2010)
20. Loh, K.P., et al.: Graphene oxide as a chemically tunable platform for optical applications. Nat. Chem 2(12), 1015–1024 (2010)
21. Chen, Y., et al.: Stable dispersions of graphene and highly conducting graphene films: a new approach to creating colloids of graphene monolayers. Chem. Commun. (Camb.) 45(30), 4527–4529 (2009)
22. Park, S., et al.: Hydrazine-reduction of graphite- and graphene oxide. Carbon. 49(9), 3019–3023 (2011)
23. Mattevi, C., et al.: Evolution of electrical, chemical, and structural properties of transparent and conducting chemically derived graphene thin films. Adv. Funct. Mater. 19(16), 2577–2583 (2009)
24. Yang, D., et al.: Chemical analysis of graphene oxide films after heat and chemical treatments by X-ay photoelectron and micro-Raman spectroscopy. Carbon. 47(1), 145–152 (2009)
25. Li, X., et al.: Simultaneous nitrogen doping and reduction of graphene oxide. J. Am. Chem. Soc. 131(43), 15939–15944 (2009)
26. Hou, W.C., et al.: Photochemical transformation of graphene oxide in sunlight. Environ. Sci. Technol. 49(6), 3435–3443 (2015)
27. Mohandoss, M., et al.: Solar mediated reduction of graphene oxide. RSC Adv. 7(2), 957–963 (2017)
28. De Silva, K.K.H., et al.: Chemical reduction of graphene oxide using green reductants. Carbon. 119, 190–199 (2017)
29. Khosroshahi, Z., et al.: Green Reduction of Graphene Oxide by Ascorbic Acid. AIP Conference Proceedings. AIP Publishing (2018). https://doi.org/10.1063/1.5018941
30. Zhou, Y., et al.: Hydrothermal dehydration for the "green" reduction of exfoliated graphene oxide to graphene and demonstration of tunable optical limiting properties. Chem. Mater. 21(13), 2950–2956 (2009)

31. Shen, Y., et al.: Evolution of the band-gap and optical properties of graphene oxide with controllable reduction level. Carbon. 62, 157–164 (2013)
32. Liu, Z.-B., et al.: Ultrafast dynamics and nonlinear optical responses from Sp2- and Sp3-hybridized domains in graphene oxide. J. Phys. Chem. Lett. 2(16), 1972–1977 (2011)
33. Ruzicka, B.A., et al.: Femtosecond pump-probe studies of reduced graphene oxide thin films. Appl. Phys. Lett. 96(17), 173106-1–173106-3 (2010)
34. Zhao, X., et al.: Ultrafast carrier dynamics and saturable absorption of solution-processable few-layered graphene oxide. Appl. Phys. Lett. 98(12), 121905-1–121905-3 (2011)
35. Marcano, D.C., et al.: Improved synthesis of graphene oxide. ACS Nano. 4(8), 4806–4814 (2010)
36. Tuinstra, F., Koenig, J.L.: Raman spectrum of graphite. J. Chem. Phys. 53(3), 1126–1130 (1970)
37. Pimenta, M.A., et al.: Studying disorder in graphite-based systems by Raman spectroscopy. Phys. Chem. Chem. Phys. 9(11), 1276–1291 (2007)
38. Boutchich, M., et al.: Characterization of graphene oxide reduced through chemical and biological processes. J. Phys. Conf., 433, 012001-1–012001-8 (2013)
39. Sakakibara, Y., et al.: Carbon nanotube-poly(vinylalcohol) nanocomposite film devices: applications for femtosecond fiber laser mode lockers and optical amplifier noise suppressors. Jpn. J. Appl. Phys. 44(4A), 1621–1625 (2005)
40. Sathiyan, S., et al.: All-normal dispersion passively mode-locked Yb-doped fiber laser using Mos2–Pva saturable absorber. Laser Phys. 26(5), 055103-1–055103-7 (2016)
41. Wu, K., et al.: Ws(2) as a saturable absorber for ultrafast photonic applications of mode-locked and Q-switched lasers. Opt. Express. 23(9), 11453–11461 (2015)
42. Garmire, E.: Resonant optical nonlinearities in semiconductors. IEEE J. Sel. Top. Quant. Electron. 6(6), 1094–1110 (2000)
43. Liang, G., et al.: Technique and model for modifying the saturable absorption (Sa) properties of 2d nanofilms by considering interband exciton recombination. J. Mater. Chem. C. 6(28), 7501–7511 (2018)
44. Hasegawa, A., Kodama, Y.: Signal transmission by optical solitons in monomode fiber. Proc. IEEE. 69(9), 1145–1150 (1981)
45. Hasegawa, A.: Soliton-based optical communications: an overview. IEEE J. Sel. Top. Quant. Electron. 6(6), 1161–1172 (2000)
46. Woodward, R.I.: Dispersion engineering of mode-locked fibre lasers. J. Optic. 20(3), 033002-1–033002-16 (2018)
47. Dennis, M.L., Duling, I.N.: Experimental study of sideband generation in femtosecond fiber lasers. IEEE J. Quant. Electron. 30(6), 1469–1477 (1994)
48. Jeon, J., Lee, J., Lee, J.H.: Numerical study on the minimum modulation depth of a saturable absorber for stable fiber laser mode locking. J. Opt. Soc. Am. B. 32(1), 31–37 (2014)

How to cite this article: Ismail MA, Abdul Razak MZ, Harun SW, Hashim AM. Reduction-controlled graphene oxide saturable absorbers and its effect on ultrashort Er-doped fibre laser. *IET Optoelectron*. 2021;15:61–68. https://doi.org/10.1049/ote2.12012

APPENDIX A1 Performance summary of samples A, B and C

Sample	Exposure time (min)	Insertion loss (dB)	Mod. depth (%)	λ_{centre} (nm)	λ (nm)	λ_{FWHM} (fs)	TBP	f_{rep} (MHz)	P_{out} (mW)
A	No reduction	2.53	0.69	1558.29	4.22	670	0.349	25.07	0.482
B	15	2.85	1.2	1557.94	4.52	580	0.324	25.18	0.434
C	30	3.05	1.94	1556.73	6.73	520	0.433	25.2	0.242

Abbreviation: FWHM, full width at half maximum; TBP, time-bandwidth product.